SCIENCE CHINA
Physics, Mechanics & Astronomy

• Research Paper •

May 2010 Vol.53 No.5: 954–965
doi: 10.1007/s11433-010-0186-y

# The complex variable reproducing kernel particle method for elasto-plasticity problems

CHEN Li[1] & CHENG YuMin[2*]

[1] *Department of Engineering Mechanics, Chang'an University, Xi'an 710064, China;*
[2] *Shanghai Institute of Applied Mathematics and Mechanics, Shanghai University, Shanghai 200072, China*

Received June 26, 2009; accepted October 27, 2009

On the basis of reproducing kernel particle method (RKPM), using complex variable theory, the complex variable reproducing kernel particle method (CVRKPM) is discussed in this paper. The advantage of the CVRKPM is that the correction function of a two-dimensional problem is formed with one-dimensional basis function when the shape function is formed. Then the CVRKPM is applied to solve two-dimensional elasto-plasticity problems. The Galerkin weak form is employed to obtain the discretized system equation, the penalty method is used to apply the essential boundary conditions. And then, the CVRKPM for two-dimensional elasto-plasticity problems is formed, the corresponding formulae are obtained, and the Newton-Raphson method is used in the numerical implementation. Three numerical examples are given to show that this method in this paper is effective for elasto-plasticity analysis.

**meshless method, reproducing kernel particle method (RKPM), complex variable reproducing kernel particle method (CVRKPM), correction function, elasto-plasticity**

**PACS:** 02.60.Cb, 02.70.-c, 02.90.+p, 46.15.-x

## 1 Introduction

Elasto-plasticity problem is one of the important problems in civil engineering, mechanical engineering, water engineering, aviation and material sciences, and so on. Under the elasto-plasticity state, the relationship of material stress and strain is nonlinear, then many difficulties occur for obtaining the solutions of elasto-plasticity problems. It is just for this reason that only a few simple elasto-plasticity problems can be solved analytically, then the numerical methods must be applied to obtain the approximate solution of elasto-plasticity problems when the solution domains are complicated. In recent years, with the development of computer technology, the numerical methods have been widely used to solve various elasto-plasticity problems of engineering structures. The finite element method (FEM) and boundary element method (BEM) are the main numerical methods to obtain the solutions of elasto-plasticity problems at present. However, these methods are based on the meshes of the solution domain, and the re-meshing technique should be carried out with a large computational cost when large deformation occurs.

Meshless methods are approximations based on nodes without initial mesh and re-meshing. Then meshless methods can overcome the disadvantage that the conventional numerical methods depend on the mesh of the solution domain [1,2]. Meshless methods have some advantages over the FEM in solving dynamic fracturing and non-linear problems. With the development of meshless methods, some researchers have successfully applied some meshless methods to the elasto-plasticity problems in recent years [3–9].

At present, some meshless methods such as the ele-

*Corresponding author (email: ymcheng@shu.edu.cn, ymcheng@sh163.net)

ment-free Galerkin (EFG) method [10], the reproducing kernel particle method (RKPM) [11], Hp-clouds meshless method [12], the finite point method [13,14], the meshless local Petrov-Galerkin (MLPG) method [15], the meshless point collocation method (PCM) [16], the wavelet particle method (WPM) [17], the meshless finite element method (MFEM) [18], the complex variable meshless method [19–21], the meshless manifold method [22,23], the meshless boundary integral equation methods [24–29], etc., have been developed.

The RKPM is developed on the basis of the smoothed particle hydrodynamics (SPH) method. The RKPM is one of the most important methods used to form approximation function in the meshless methods. As the earliest meshless method, the SPH method was used to solve infinite field problems. For finite field problems, the SPH method leads to low computational accuracy and unstability because the compatibility conditions on the boundary can not be satisfied. To overcome the disadvantages of the SPH method for solving a finite domain problem, Liu et al. proposed the RKPM by introducing a corrected function to integral transformation in the SPH method to satisfy the boundary compatibility, and the unstability of the SPH method can be eliminated [11].

Compared with conventional numerical methods, the RKPM has many advantages, such as good smoothness and high computational accuracy, and that the shape function is formed without meshes. But the RKPM has a great computational cost because of a great number of nodes selected in the domain of a problem. To overcome the disadvantage which the RKPM has a great computational cost, the complex variables reproducing kernel particle method (CVRKPM) was presented by the authors of this paper [30]. The advantages of the CVRKPM are that the correction function of a 2D problem is formed with 1D basis function when the shape function is obtained, which lead to the fewer nodes selected in the domain of the problem without the loss of the computational accuracy, then the computational cost is reduced.

In this paper, the CVRKPM for two-dimensional elasto-plasticity is proposed. For the non-linear elasto-plasticity problems, the incremental CVRKPM is used to obtain field variable approximation, and the increments of stress and strain are used to characterize the elasto-plastic constitutive relationship. And the penalty method is employed to apply the essential boundary conditions. And then based on the incremental constitutive relationship, the control equation of the CVRKPM is obtained. The Newton-Raphson method is used in the numerical implementation. The CVRKPM in this paper can analyze the elasto-plasticity behaviors and some characteristics of loading and deformation history conveniently. Finally, some numerical examples are given to demonstrate the efficiency of the method in this paper.

## 2 The shape function of the CVRKPM

Consider a complex function $\overline{u}(z)$ which with the continuous derivative function defined in the domain $\Omega$. In the CVRKPM, the key to obtain the trial function is using the corrected kernel function $\overline{w}_h(z-z')$ to form the reproducing kernel approximation $\overline{u}^h(z)$ of the function $\overline{u}(z)$ at point $z$, and

$$\begin{aligned}\overline{u}^h(z) = u_1^h(z) + \mathrm{i}u_2^h(z) = \int_{\Omega} \overline{u}(z') \cdot \overline{w}_h(z-z') \cdot \mathrm{d}z', \\ (z = x_1 + \mathrm{i}x_2 \in \Omega),\end{aligned} \tag{1}$$

where $\overline{w}_h(z-z')$ is a corrected reproducing kernel function:

$$\overline{w}_h(z-z') = C(z; z-z') \cdot w_h(z-z'), \tag{2}$$

where $w_h(z-z')$ is the kernel function which has a compact support domain, and $C(z;z-z')$ is the correction function which is expressed as a linear combination of polynomial basis functions, i.e.

$$\begin{aligned}C(z; z-z') &= \sum_{i=0}^{m} p_i(z-z') \cdot b_i(z) \\ &= \boldsymbol{p}^{\mathrm{T}}(z-z')\boldsymbol{b}(z), \quad (z \in \Omega),\end{aligned} \tag{3}$$

$$\boldsymbol{p}^{\mathrm{T}}(z-z') = \big(p_0(z-z'),\, p_1(z-z'),\, \cdots,\, p_m(z-z')\big), \tag{4}$$

$$\boldsymbol{b}^{\mathrm{T}}(z) = \big(b_0(z),\, b_1(z),\, \cdots,\, b_m(z)\big), \tag{5}$$

where $m$ is the highest order of polynomial basis functions, $p_i(z-z')$ are the basis functions, and $b_i(z)$ are the corresponding coefficients. In general, for two-dimensional problems, the basis functions can be chosen as linear basis

$$\boldsymbol{p}^{\mathrm{T}} = \big(1,\ z-z'\big), \tag{6}$$

or quadratic basis

$$\boldsymbol{p}^{\mathrm{T}} = \big(1,\ z-z',\ (z-z')^2\big). \tag{7}$$

The discretized form of the complex variables reproducing kernel approximation can be obtained by applying the trapezoidal rule to eq. (1), i.e.

$$\begin{aligned}\overline{u}^h(z) &= \sum_{I=1}^{n} \overline{u}(z_I) \cdot \overline{w}_h(z-z_I) \cdot \Delta V_I \\ &= \sum_{I=1}^{n} C(z; z-z_I) \cdot w_h(z-z_I) \cdot \Delta V_I \cdot \overline{u}(z_I),\end{aligned} \tag{8}$$

where $z_I$ is the node in the support domain of $z$, $n$ is the total number of the nodes in the support domain of $z$,

$$\overline{u}(z_I) = u_1(z_I) + \mathrm{i}u_2(z_I), \tag{9}$$

and $\Delta V_I$ is the volume of node $z_I$ and represents the integration weight, i.e.

$$\sum_{I=1}^{n_t} \Delta V_I = \Omega, \tag{10}$$

where $n_t$ is the total number of nodes distributed in the solution domain.

Eq. (8) can be rewritten as

$$\overline{u}^h(z) = \boldsymbol{C}(z)\boldsymbol{W}(z)\boldsymbol{V}\cdot\overline{\boldsymbol{u}}, \tag{11}$$

where

$$\overline{\boldsymbol{u}} = \left(\overline{u}(z_1),\ \overline{u}(z_2),\ \cdots,\ \overline{u}(z_n)\right)^{\mathrm{T}} = Q\boldsymbol{u}, \tag{12}$$

$$\boldsymbol{u} = \left(u_1(z_1),\ u_2(z_1),\ u_1(z_2), u_2(z_2),\ \cdots,\ u_1(z_n),\ u_2(z_n)\right)^{\mathrm{T}}, \tag{13}$$

$$Q = \begin{bmatrix} 1 & i & 0 & 0 & 0 & 0 & \cdots & 0 & 0 \\ 0 & 0 & 1 & i & 0 & 0 & \cdots & 0 & 0 \\ 0 & 0 & 0 & 0 & 1 & i & \cdots & 0 & 0 \\ \vdots & \vdots & \vdots & \vdots & \vdots & \vdots & \ddots & \vdots & \vdots \\ 0 & 0 & 0 & 0 & 0 & 0 & \cdots & 1 & i \end{bmatrix}_{n\times 2n}, \tag{14}$$

$$\boldsymbol{W}(z) = \begin{bmatrix} w_h(z-z_1) & 0 & \cdots & 0 \\ 0 & w_h(z-z_2) & \cdots & 0 \\ \vdots & \vdots & \ddots & \vdots \\ 0 & 0 & \cdots & w_h(z-z_n) \end{bmatrix}, \tag{15}$$

$$\boldsymbol{V} = \begin{bmatrix} \Delta V_1 & 0 & \cdots & 0 \\ 0 & \Delta V_2 & \cdots & 0 \\ \vdots & \vdots & \ddots & \vdots \\ 0 & 0 & \cdots & \Delta V_n \end{bmatrix}. \tag{16}$$

Let

$$C_I(z) = C(z; z-z_I) = \boldsymbol{p}^{\mathrm{T}}(z-z_I)\boldsymbol{b}(z). \tag{17}$$

Then we have

$$\boldsymbol{C}(z) = \left(C_1(z),\ C_2(z), \cdots,\ C_n(z)\right) = \boldsymbol{b}^{\mathrm{T}}(z)\boldsymbol{P}, \tag{18}$$

where

$$\boldsymbol{P} = \begin{bmatrix} p_0(z-z_1) & p_0(z-z_2) & \cdots & p_0(z-z_n) \\ p_1(z-z_1) & p_1(z-z_2) & \cdots & p_1(z-z_n) \\ \vdots & \vdots & \ddots & \vdots \\ p_m(z-z_1) & p_m(z-z_2) & \cdots & p_m(z-z_n) \end{bmatrix}, \tag{19}$$

$$\boldsymbol{b}^{\mathrm{T}}(z) = \left(b_0(z),\ b_1(z),\ \cdots,\ b_m(z)\right). \tag{20}$$

Here the correction coefficients are obtained via the reproducing conditions of the trial function, and

$$\boldsymbol{M}(z)\cdot\boldsymbol{b}(z) = \boldsymbol{H}, \tag{21}$$

where

$$\boldsymbol{M}(z) = \sum_{I=1}^{n} \boldsymbol{p}(z-z_I)\cdot\boldsymbol{p}^{\mathrm{T}}(z-z_I)\cdot w_h(z-z_I)\cdot\Delta V_I, \tag{22}$$

$$\boldsymbol{H} = \left(1,\ 0,\ \cdots,\ 0\right)^{\mathrm{T}}, \tag{23}$$

$$\boldsymbol{b}(z) = \boldsymbol{M}^{-1}(z)\cdot\boldsymbol{H}. \tag{24}$$

Then the expression of the trial function $\overline{u}^h(z)$ can be written as

$$\overline{u}^h(z) = \boldsymbol{\Phi}(z)\overline{\boldsymbol{u}} = \sum_{I=1}^{n} \Phi_I(z)\overline{u}(z_I), \tag{25}$$

where $\boldsymbol{\Phi}(z)$ is defined as the shape function of the CVRKPM, and

$$\boldsymbol{\Phi}(z) = \left(\Phi_1(z),\ \Phi_2(z),\ \cdots,\ \Phi_n(z)\right) = \boldsymbol{C}(z)\cdot\boldsymbol{W}(z)\cdot\boldsymbol{V}, \tag{26}$$

$$u_1^h(z) = \mathrm{Re}[\boldsymbol{\Phi}(z)\overline{\boldsymbol{u}}] = \mathrm{Re}\left[\sum_{I=1}^{n} \Phi_I(z)\overline{u}(z_I)\right], \tag{27}$$

$$u_2^h(z) = \mathrm{Im}[\boldsymbol{\Phi}(z)\overline{\boldsymbol{u}}] = \mathrm{Im}\left[\sum_{I=1}^{n} \Phi_I(z)\overline{u}(z_I)\right]. \tag{28}$$

The advantage of the CVRKPM is that the correction function of a two-dimensional problem is formed with one-dimensional basis function, which leads to the fact that fewer nodes can be selected in the meshless method formed with the CVRKPM under the same precision. As for an arbitrary node, when its shape function and its derivatives are calculated, it is necessary to obtain the inversion of the matrix $\boldsymbol{M}$. Under the same precision, because the fewer unknown coefficients needed in the CVRKPM approximation lead to reducing the dimension of the matrix $\boldsymbol{M}$, then the CVRKPM has greater computational efficiency compared with the RKPM. For example, for the linear basis, the basis function in the RKPM is $\boldsymbol{p}^{\mathrm{T}} = \left(1,\ x_1 - x_1',\ x_2 - x_2'\right)$, and three unknown coefficients are needed; and the basis function in the CVRKPM is $\boldsymbol{p}^{\mathrm{T}} = \left(1,\ z - z'\right)$, and two unknown coefficients are needed. For the quadratic basis, the basis function in the RKPM is

$$\boldsymbol{p}^{\mathrm{T}} = \left(1,\ x_1 - x_1',\ x_2 - x_2',\ (x_1 - x_1')^2,\right.$$
$$\left.(x_1 - x_1')(x_2 - x_2'),\ (x_2 - x_2')^2\right),$$

and six unknown coefficients are needed; and the basis function in the CVRKPM is $\boldsymbol{p}^{\mathrm{T}} = \left(1,\ z - z',\ (z - z')^2\right)$, and three unknown coefficients are needed. Then for an arbitrary point in the domain, we need fewer nodes with support domains that cover the point, and thus we also require fewer nodes in the whole domain. In addition, under the same node distribution in the problem domain, the

CVRKPM has greater precision than the RKPM.

## 3 The CVRKPM for elasto-plasticity problems

### 3.1 Basic equations of elasto-plasticity problems

Because of the nonlinearity of an elasto-plasticity boundary-value problem of the structures, it is more complicated than a linear elasticity problem. When the structure works in the plastic state, its stress-strain relationship appears to be nonlinear, then the control equation and boundary conditions can be in the increment form, and the symbol ' • ' denotes the increment form of a variable. And the plastic item should be considered. Suppose the structure via a loading history, the displacement $\boldsymbol{u}$, strain $\boldsymbol{\varepsilon}$ and stress $\boldsymbol{\sigma}$ at time $t$ have been obtained. If the body force rate $\dot{\boldsymbol{b}}$, the traction rate $\dot{\bar{\boldsymbol{t}}}$ on the natural boundary $\Gamma_t$ and velocity distribution $\dot{\bar{\boldsymbol{u}}}$ on the essential boundary $\Gamma_u$ are given, then the equilibrium equation for elasto-plasticity problems can be written as

$$\boldsymbol{L}^{\mathrm{T}}\dot{\boldsymbol{\sigma}}+\dot{\boldsymbol{b}}=0\text{, in }\Omega, \tag{29}$$

where $\boldsymbol{L}$ is differential operator matrix, i.e.

$$\boldsymbol{L}=\begin{bmatrix}\dfrac{\partial}{\partial x_1} & 0\\ 0 & \dfrac{\partial}{\partial x_2}\\ \dfrac{\partial}{\partial x_2} & \dfrac{\partial}{\partial x_1}\end{bmatrix}. \tag{30}$$

The strain-displacement relationship can be written as

$$\dot{\boldsymbol{\varepsilon}}=\boldsymbol{L}\dot{\boldsymbol{u}}\text{, in }\Omega. \tag{31}$$

The stress-strain relationship can be expressed as

$$\dot{\boldsymbol{\sigma}}=\boldsymbol{D}\dot{\boldsymbol{\varepsilon}}, \tag{32}$$

where $D$ is material constant matrix:

$$\boldsymbol{D}=[D]_{\mathrm{e}}=\frac{E}{1-v^2}\begin{bmatrix}1 & v & 0\\ v & 1 & 0\\ 0 & 0 & \dfrac{1-v}{2}\end{bmatrix} \tag{33}$$

in the elastic state, and

$$\boldsymbol{D}=[D]_{\mathrm{ep}} \tag{34}$$

in the plastic state. $[D]_{\mathrm{ep}}$ is the elasto-plasticity matrix of increment theory, i.e.

$$[D]_{\mathrm{ep}}=\frac{E}{Q}\begin{bmatrix}\sigma_{22}'^{\,2}+2P & -\sigma_{11}'\sigma_{22}'+2vP & -\dfrac{\sigma_{11}'+v\sigma_{22}'}{1+v}\sigma_{12}\\ -\sigma_{11}'\sigma_{22}'+2vP & \sigma_{11}'+2P & -\dfrac{\sigma_{22}'+v\sigma_{11}'}{1+v}\sigma_{12}\\ -\dfrac{\sigma_{11}'+v\sigma_{22}'}{1+v}\sigma_{12} & -\dfrac{\sigma_{22}'+v\sigma_{11}'}{1+v}\sigma_{12} & \dfrac{R}{2(1+v)}+\dfrac{2H'}{9E}(1-v)\bar{\sigma}^2\end{bmatrix}, \tag{35}$$

where $E$ is Young's modulus, $v$ is Poisson's ratio, and $H'$ is the plastic modulus for material hardening, and determined by the relationship of stress and plastic strain obtained from the material tests:

$$H'=\frac{\mathrm{d}\sigma}{\mathrm{d}\varepsilon_p}=\frac{f'}{1-\dfrac{f'}{E}}=\frac{EE'}{E-E'}, \tag{36}$$

where $f'=\dfrac{\mathrm{d}\sigma}{\mathrm{d}\varepsilon}=E'$, $E'$ is known as tangent modulus.

In eq. (35):

$$P=\frac{2H'}{9E}\bar{\sigma}^2+\frac{\sigma_{12}^2}{1+v}, \tag{37}$$

$$R=\sigma_{11}'^{\,2}+2v\sigma_{11}'\sigma_{22}'+\sigma_{22}'^{\,2}, \tag{38}$$

$$Q=R+2(1-v^2)P, \tag{39}$$

where $\bar{\sigma}$ is the equivalent stress, $\sigma_{11}'$ and $\sigma_{22}'$ are the deviatoric stresses, and we have:

$$\bar{\sigma}=\sqrt{\sigma_{11}^2+\sigma_{22}^2-\sigma_{11}\sigma_{22}+3\sigma_{12}^2}, \tag{40}$$

$$\begin{cases}\sigma_{11}'=\sigma_{11}-\dfrac{\sigma_{11}+\sigma_{22}}{3},\\ \sigma_{22}'=\sigma_{22}-\dfrac{\sigma_{11}+\sigma_{22}}{3}.\end{cases} \tag{41}$$

As for the plane strain problems, when the structure is in plasticity state, Poisson's ratio $v=0.5$. For the corresponding elasto-plasticity matrix, $E$ in $[D]_{\mathrm{ep}}$ of plane stress problems is only changed into $\dfrac{E}{1-v^2}$, and $v$ is changed into $\dfrac{v}{1-v}$.

The boundary conditions can be written as:

$$\dot{\boldsymbol{u}}=\dot{\bar{\boldsymbol{u}}},\ \text{on}\ \Gamma_u, \tag{42}$$

$$\boldsymbol{n}\cdot\dot{\boldsymbol{\sigma}}=\dot{\bar{\boldsymbol{t}}},\ \text{on}\ \Gamma_t, \tag{43}$$

where $\dot{\bar{\boldsymbol{u}}}$ is the prescribed velocity distribution at an arbi-

trary point $z$ on the essential boundary $\Gamma_u$; $\dot{\bar{t}}$ is the prescribed traction rate at an arbitrary point $z$ on the natural boundary $\Gamma_t$; $\Gamma$ is the boundary of the domain $\Omega$, and $\Gamma = \Gamma_u \cup \Gamma_t$, $\Gamma_u \cap \Gamma_t = \varnothing$; $n_1$ and $n_2$ are the units outward normal to the boundary $\Gamma_t$, respectively, and we have

$$\boldsymbol{n} = \begin{bmatrix} n_1 & 0 & n_2 \\ 0 & n_2 & n_1 \end{bmatrix}. \tag{44}$$

### 3.2 Galerkin weak form for elasto-plasticity problems

In this paper, the penalty method is used to enforce the essential boundary conditions. The corresponding constrained Galerkin weak form can be obtained as follows [6]:

$$\int_\Omega \delta\dot{\boldsymbol{\varepsilon}}^{\mathrm{T}} \dot{\boldsymbol{\sigma}} \mathrm{d}\Omega - \int_\Omega \delta\dot{\boldsymbol{u}}^{\mathrm{T}} \dot{\boldsymbol{b}} \mathrm{d}\Omega - \int_{\Gamma_t} \delta\dot{\boldsymbol{u}}^{\mathrm{T}} \dot{\bar{\boldsymbol{t}}} \mathrm{d}\Gamma + \alpha \int_{\Gamma_u} \delta\dot{\boldsymbol{u}}^{\mathrm{T}} \boldsymbol{S}(\dot{\boldsymbol{u}} - \dot{\bar{\boldsymbol{u}}}) \mathrm{d}\Gamma = 0, \tag{45}$$

where $\alpha$ is penalty factor which is assigned the constant of a large positive number. At present, the following equation is adopted to determine the penalty factor mostly:

$$\alpha = (1.0\times10^3 \sim 1.0\times10^5)\times E, \tag{46}$$

$$\boldsymbol{S} = \begin{bmatrix} s_1 & 0 \\ 0 & s_2 \end{bmatrix}. \tag{47}$$

When the displacement exists at the boundary at $x_1$ (or $x_2$) direction, the corresponding $s_1$ (or $s_2$) equals to 1, otherwise to 0.

By using the strain-displacement relationship eq. (31) and the stress-strain relationship eq. (32), eq. (45) can be explicitly expressed as:

$$\int_\Omega \delta(\boldsymbol{L}\dot{\boldsymbol{u}})^{\mathrm{T}} \boldsymbol{D}(\boldsymbol{L}\dot{\boldsymbol{u}}) \mathrm{d}\Omega - \int_\Omega \delta\dot{\boldsymbol{u}}^{\mathrm{T}} \dot{\boldsymbol{b}} \mathrm{d}\Omega - \int_{\Gamma_t} \delta\dot{\boldsymbol{u}}^{\mathrm{T}} \dot{\bar{\boldsymbol{t}}} \mathrm{d}\Gamma + \alpha \int_{\Gamma_u} \delta\dot{\boldsymbol{u}}^{\mathrm{T}} \boldsymbol{S}(\dot{\boldsymbol{u}} - \dot{\bar{\boldsymbol{u}}}) \mathrm{d}\Gamma = 0. \tag{48}$$

### 3.3 The discrete equation of the CVRKPM for elasto-plasticity problems

From the CVRKPM approximation (25), the velocity $\dot{\bar{u}}(z)$ at an arbitrary point $z$ in the domain can be expressed as follows:

$$\dot{\bar{u}}(z) = \dot{u}_1(z) + \mathrm{i}\dot{u}_2(z) = \boldsymbol{\Phi}(z)\dot{\bar{\boldsymbol{u}}} = \sum_{I=1}^{n} \Phi_I(z)\dot{\bar{u}}(z_I), \tag{49}$$

where $\boldsymbol{\Phi}(z)$ is the shape function, and

$$\dot{\bar{u}}(z_I) = \dot{u}_1(z_I) + \mathrm{i}\dot{u}_2(z_I). \tag{50}$$

Combining eqs. (49) and (50), we have

$$\dot{\boldsymbol{u}}(z) = \begin{pmatrix} \dot{u}_1(z) \\ \dot{u}_2(z) \end{pmatrix} = \sum_I^n \begin{bmatrix} \mathrm{Re}[\Phi_I(z)] & -\mathrm{Im}[\Phi_I(z)] \\ \mathrm{Im}[\Phi_I(z)] & \mathrm{Re}[\Phi_I(z)] \end{bmatrix} \cdot \begin{pmatrix} \dot{u}_1(z_I) \\ \dot{u}_2(z_I) \end{pmatrix} = \sum_I^n \tilde{\boldsymbol{\Phi}}_I(z)\cdot\dot{\boldsymbol{u}}_I = \tilde{\boldsymbol{\Phi}}(z)\cdot\dot{\boldsymbol{U}}, \tag{51}$$

where $\tilde{\boldsymbol{\Phi}}(z)$ is the matrix of shape functions, $n$ is the number of nodes in the support domain of point $z$, and $\dot{\boldsymbol{U}}$ is nodal velocity vector, and

$$\tilde{\boldsymbol{\Phi}}(z) = \left(\tilde{\boldsymbol{\Phi}}_1(z),\ \tilde{\boldsymbol{\Phi}}_2(z),\ \cdots,\ \tilde{\boldsymbol{\Phi}}_n(z)\right), \tag{52}$$

$$\tilde{\boldsymbol{\Phi}}_I(\mathrm{z}) = \begin{bmatrix} \mathrm{Re}[\Phi_I(z)] & -\mathrm{Im}[\Phi_I(z)] \\ \mathrm{Im}[\Phi_I(z)] & \mathrm{Re}[\Phi_I(z)] \end{bmatrix}, \tag{53}$$

$$\dot{\boldsymbol{U}}^{\mathrm{T}} = \left(\dot{\boldsymbol{u}}^{\mathrm{T}}(z_1), \dot{\boldsymbol{u}}^{\mathrm{T}}(z_2), \cdots, \dot{\boldsymbol{u}}^{\mathrm{T}}(z_n)\right). \tag{54}$$

The product of $\boldsymbol{L}\dot{\boldsymbol{u}}$ in eq. (48) can be expressed as follows:

$$\boldsymbol{L}\dot{\boldsymbol{u}} = \boldsymbol{L}\sum_I^n \tilde{\boldsymbol{\Phi}}_I(z)\dot{\boldsymbol{u}}_I = \sum_I^n \boldsymbol{L}\tilde{\boldsymbol{\Phi}}_I(z)\dot{\boldsymbol{u}}_I = \sum_I^n \boldsymbol{B}_I(z)\dot{\boldsymbol{u}}_I = \boldsymbol{B}(z)\cdot\dot{\boldsymbol{U}}, \tag{55}$$

where

$$\boldsymbol{B}(z) = \left(\boldsymbol{B}_1(z),\ \boldsymbol{B}_2(z),\ \cdots,\ \boldsymbol{B}_n(z)\right), \tag{56}$$

$$\boldsymbol{B}_I(z) = \begin{bmatrix} \mathrm{Re}[\Phi_{I,1}(z)] & -\mathrm{Im}[\Phi_{I,1}(z)] \\ \mathrm{Im}[\Phi_{I,2}(z)] & \mathrm{Re}[\Phi_{I,2}(z)] \\ \mathrm{Re}[\Phi_{I,2}(z)] + \mathrm{Im}[\Phi_{I,1}(z)] & -\mathrm{Im}[\Phi_{I,2}(z)] + \mathrm{Re}[\Phi_{I,1}(z)] \end{bmatrix}. \tag{57}$$

Substituting eqs. (51) and (55) into eq. (48) yields

$$\int_\Omega \delta\dot{\boldsymbol{U}}^{\mathrm{T}}(\boldsymbol{B}^{\mathrm{T}}\cdot\boldsymbol{D}\cdot\boldsymbol{B})\dot{\boldsymbol{U}}\mathrm{d}\Omega - \int_\Omega \delta\dot{\boldsymbol{U}}^{\mathrm{T}}\tilde{\boldsymbol{\Phi}}^{\mathrm{T}}\dot{\boldsymbol{b}}\mathrm{d}\Omega - \int_{\Gamma_t} \delta\dot{\boldsymbol{U}}^{\mathrm{T}}\tilde{\boldsymbol{\Phi}}^{\mathrm{T}}\dot{\bar{\boldsymbol{t}}}\mathrm{d}\Gamma + \alpha\int_{\Gamma_u} \delta\dot{\boldsymbol{U}}^{\mathrm{T}}(\tilde{\boldsymbol{\Phi}}^{\mathrm{T}}\cdot\boldsymbol{S}\cdot\tilde{\boldsymbol{\Phi}})\dot{\boldsymbol{U}}\mathrm{d}\Gamma + \alpha\int_{\Gamma_u} \delta\dot{\boldsymbol{U}}^{\mathrm{T}}(\tilde{\boldsymbol{\Phi}}^{\mathrm{T}}\cdot\boldsymbol{S}\cdot\dot{\bar{\boldsymbol{u}}})\mathrm{d}\Gamma = 0. \tag{58}$$

Because the nodal test function $\delta\dot{\boldsymbol{U}}^{\mathrm{T}}$ is arbitrary, we can obtain the final discretized equation as follows:

$$(\boldsymbol{K} + \boldsymbol{K}^{\alpha})\dot{\boldsymbol{U}} = \dot{\boldsymbol{F}} + \dot{\boldsymbol{F}}^{\alpha}, \tag{59}$$

where

$$\boldsymbol{K} = \int_\Omega \boldsymbol{B}^{\mathrm{T}}\cdot\boldsymbol{D}\cdot\boldsymbol{B}\mathrm{d}\Omega, \tag{60}$$

$$\dot{\boldsymbol{F}} = \int_{\Omega} \tilde{\boldsymbol{\Phi}}^{\mathrm{T}} \dot{\boldsymbol{b}} \mathrm{d}\Omega + \int_{\Gamma_t} \tilde{\boldsymbol{\Phi}}^{\mathrm{T}} \dot{\bar{\boldsymbol{t}}} \mathrm{d}\Gamma, \tag{61}$$

$$\boldsymbol{K}^{\alpha} = \alpha \int_{\Gamma_u} \tilde{\boldsymbol{\Phi}}^{\mathrm{T}} \cdot \boldsymbol{S} \cdot \tilde{\boldsymbol{\Phi}} \mathrm{d}\Gamma, \tag{62}$$

$$\dot{\boldsymbol{F}}^{\alpha} = \alpha \int_{\Gamma_u} \tilde{\boldsymbol{\Phi}}^{\mathrm{T}} \cdot \boldsymbol{S} \cdot \dot{\bar{\boldsymbol{u}}} \mathrm{d}\Gamma. \tag{63}$$

Let

$$\bar{\boldsymbol{K}} = \boldsymbol{K} + \boldsymbol{K}^{\alpha}, \tag{64}$$

$$\dot{\bar{\boldsymbol{F}}} = \dot{\boldsymbol{F}} + \dot{\boldsymbol{F}}^{\alpha}, \tag{65}$$

eq. (59) can be simply written as

$$\bar{\boldsymbol{K}} \dot{\boldsymbol{U}} = \dot{\bar{\boldsymbol{F}}}. \tag{66}$$

If the concentrated force $\hat{\boldsymbol{T}}$ is applied to a certain point $z_0$ on the boundary $\Gamma_t$ and the concentrated force rate $\dot{\hat{\boldsymbol{T}}}$ can be given as

$$\dot{\hat{\boldsymbol{T}}}(z_0) = \left( \dot{\hat{T}}_1(z_0),\ \dot{\hat{T}}_2(z_0) \right)^{\mathrm{T}}. \tag{67}$$

Similar to the elastic problems, the contribution of the concentrated force to equivalent node load increment can be given as [30]

$$\tilde{\boldsymbol{\Phi}}^{\mathrm{T}}(z_0) \cdot \dot{\hat{\boldsymbol{T}}}(z_0) \to \dot{\bar{\boldsymbol{F}}}. \tag{68}$$

Therefore, in the case of existence of body force, traction and concentrated force, the equivalent node load increment can be expressed as follows:

$$\dot{\bar{\boldsymbol{F}}} = \int_{\Omega} \tilde{\boldsymbol{\Phi}}^{\mathrm{T}} \dot{\boldsymbol{b}} \mathrm{d}\Omega + \int_{\Gamma_t} \tilde{\boldsymbol{\Phi}}^{\mathrm{T}} \dot{\bar{\boldsymbol{t}}} \mathrm{d}\Gamma + \tilde{\boldsymbol{\Phi}}^{\mathrm{T}}(z_0) \cdot \dot{\hat{\boldsymbol{T}}}(z_0) + \alpha \int_{\Gamma_u} \tilde{\boldsymbol{\Phi}}^{\mathrm{T}} \boldsymbol{S} \dot{\bar{\boldsymbol{u}}} \mathrm{d}\Gamma, \tag{69}$$

this is the CVRKPM for elasto-plasticity problems.

## 4 Solution to the elasto-plasticity problems—Increment tangent stiffness matrix method

### 4.1 Linearization of nonlinear problems

For the elasto-plasticity problem with small deformation, the displacement is continuous, and the relationship of displacement and strain is linear, but the relationship of stress and strain in the plastic field is nonlinear. When the loading has a minor increment, the nonlinear relationship between the stress differentiation and strain differentiation should be adopted.

In order to solve the nonlinear problem, in this paper we convert it into a series of linear problems using the method of gradually increasing loading. In certain stress and strain level, increasing a load increment, we will obtain the stress increment $\Delta\boldsymbol{\sigma}$ and strain increment $\Delta\boldsymbol{\varepsilon}$. Only when the load increment is rightly small, the stress and strain differentiation can be replaced by their increments, and then the relationship between the stress increment and strain increment can be expressed approximately as follows:

$$\Delta\boldsymbol{\sigma} = \left[D\right]_{\mathrm{ep}} \Delta\boldsymbol{\varepsilon}, \tag{70}$$

where $\left[D\right]_{\mathrm{ep}}$ is only related to the stress before adding the load increment, but not related to the stress and strain increments after adding the load increment. Then eq. (70) is a linear equation system. Thus for the load increment at each step, similar to elasticity problems entirely, we can form the corresponding formulae to obtain the displacement increment, strain increment and stress increment produced by the load increment in this step. And then, the previous stress state is revised, and the calculation for the load increment at the next step will begin. The problem with each load increment should be a linear problem, and then the solution of the elasto-plasticity problem will be obtained.

First of all, the linear elasticity analysis should be made to obtain the structure displacement, strain and stress under the elastic limit load $\bar{\boldsymbol{F}}_0$, and they are recorded as $\boldsymbol{U}_0$, $\boldsymbol{\varepsilon}_0$ and $\boldsymbol{\sigma}_0$ respectively. And then, the structure will enter the yield state, the load will be added with load increment method, and the corresponding node load increment $\Delta\bar{\boldsymbol{F}}_1$ and the corresponding stiffness matrix can be obtained. When obtaining the stiffness matrix, for Gaussian quadrature points entering the yield state, we must use $\left[D\right]_{\mathrm{ep}}$ to replace $\left[D\right]_{\mathrm{e}}$, and the stress in $\left[D\right]_{\mathrm{ep}}$ should be $\boldsymbol{\sigma}_0$. And then the stiffness matrix is related to the stress before adding the load increment, and it is recorded as $\bar{\boldsymbol{K}}(\boldsymbol{\sigma}_0)$.

Solving the equation

$$\bar{\boldsymbol{K}}(\boldsymbol{\sigma}_0) \cdot \Delta\boldsymbol{U}_1 = \Delta\bar{\boldsymbol{F}}_1, \tag{71}$$

then $\Delta\boldsymbol{U}_1$, $\Delta\boldsymbol{\varepsilon}_1$ and $\Delta\boldsymbol{\sigma}_1$ can be obtained, and then the displacement, strain and stress after a load increment are obtained. Therefore we have obtained a new stress $\boldsymbol{\sigma}_1 = \boldsymbol{\sigma}_0 + \Delta\boldsymbol{\sigma}_1$. The rest can be deduced by analogy. After $i-1$ load increments, the displacement, strain and stress at that time can be obtained, and the stress is $\boldsymbol{\sigma}_{i-1}$. When the *i*th load increment $\Delta\bar{\boldsymbol{F}}_i$ is added, solving the following equation:

$$\bar{\boldsymbol{K}}(\boldsymbol{\sigma}_{i-1}) \cdot \Delta\boldsymbol{U}_i = \Delta\bar{\boldsymbol{F}}_i, \tag{72}$$

we can get the *i*-th displacement increment $\Delta\boldsymbol{U}_i$, strain increment $\Delta\boldsymbol{\varepsilon}_i$ and stress increment $\Delta\boldsymbol{\sigma}_i$, and then the

new stress can be obtained, i.e.

$$\boldsymbol{\sigma}_i = \boldsymbol{\sigma}_{i-1} + \Delta\boldsymbol{\sigma}_i. \tag{73}$$

Repeating the above mentioned process until the load of the problem is added completely, the displacement, strain and stress of the elasto-plasticity problem can be obtained.

### 4.2 Formation of the stiffness matrix $\bar{\boldsymbol{K}}(\boldsymbol{\sigma}_{i-1})$

When using increment tangent stiffness matrix method to analyze an elasto-plasticity problem, we must obtain the stiffness matrix and stress at each load increment step.

From eq. (64) we can obtain the stiffness matrix. In eq. (64), $\boldsymbol{K}(\boldsymbol{\sigma}_{i-1}) = \int_{\Omega} \boldsymbol{B}^{\mathrm{T}} \cdot \boldsymbol{D} \cdot \boldsymbol{B} \mathrm{d}\Omega$ is the integration in the whole domain, and then use Gaussian quadrature, we have

$$\begin{aligned} K_{IJ}(\boldsymbol{\sigma}_{i-1}) &= \int_{\Omega} \boldsymbol{B}_I{}^{\mathrm{T}} \cdot \boldsymbol{D} \cdot \boldsymbol{B}_J \mathrm{d}\Omega \\ &= \sum_{i}^{n_G} w_{\mathrm{G}i} \cdot \boldsymbol{B}_I{}^{\mathrm{T}}(z_i) \cdot \boldsymbol{D}(z_i) \cdot \boldsymbol{B}_J(z_i), \end{aligned} \tag{74}$$

where $n_{\mathrm{G}}$ is the total number of Gaussian quadrature points which fall in the field intersection of support domains of node $z_I$ and $z_J$, $w_{\mathrm{G}i}$ is the integration weight of the Gaussian quadrature point $z_i$.

As for the elasto-plasticity problem, in the solution domain, a plastic zone will occur and develop with the increase of load increments. And then the stress-strain relationship at Gaussian quadrature points in the plastic zone is nonlinear. Thus, before a load increment is added at each load step, it is necessary to discuss the stress at each Gaussian quadrature point after the previous load increment step, and then the equivalent stress of the point will be obtained. If the equivalent stress at a Gaussian quadrature point is larger than the material yield stress, the Gaussian quadrature point will enter into the plastic zone, and then $\boldsymbol{D}(z_i) = [D]_{\mathrm{ep}}$, otherwise $\boldsymbol{D}(z_i) = [D]_{\mathrm{e}}$.

### 4.3 Calculation of the equivalent node load vector $\bar{\boldsymbol{F}}$

When the equivalent node load increment $\Delta\bar{\boldsymbol{F}}$ is applied, some Gaussian quadrature points in the elastic state will enter into the plastic state, and then we have $\boldsymbol{D}(z_i) = [D]_{\mathrm{e}}$. Thus, when obtaining the equivalent node load increment, the previous loading imbalance should be corrected, and then the solution will have good accuracy. Therefore, for each load increment step, the discrete increment equation system eq. (72) should be revised as follows:

$$\Delta\boldsymbol{U}_i = [\bar{\boldsymbol{K}}(\boldsymbol{\sigma}_{i-1})]^{-1} \cdot \left( \bar{\boldsymbol{F}}_i - \int_{\Omega} \boldsymbol{B}^{\mathrm{T}} \boldsymbol{\sigma}_{i-1} \mathrm{d}\Omega \right), \tag{75}$$

where the integration $\int_{\Omega} \boldsymbol{B}^{\mathrm{T}} \boldsymbol{\sigma}_{i-1} \mathrm{d}\Omega$ is the equivalent node load to the stress after the previous load increment step, and $\bar{\boldsymbol{F}}_i$ is the total equivalent node load after this load increment, i.e.

$$\bar{\boldsymbol{F}}_i = \bar{\boldsymbol{F}}_0 + \Delta\bar{\boldsymbol{F}}_1 + \Delta\bar{\boldsymbol{F}}_2 + \cdots + \Delta\bar{\boldsymbol{F}}_i. \tag{76}$$

In the practical numerical process, all the loading should be applied on the structure first, and the structure is analyzed with linear elasticity theory, and then the total equivalent node load $\bar{\boldsymbol{F}}$ is obtained from eq. (69). The equivalent node load $\frac{1}{L}\bar{\boldsymbol{F}}$, where $L = \frac{\bar{\sigma}_{\max}}{\sigma_s}$, can be used as the elastic limit load $\bar{\boldsymbol{F}}_0$. And the corresponding displacement, strain and stress under the elastic limit load can be obtained with linear elastic analysis. And then the step loading should be adopted, and $\Delta\bar{\boldsymbol{F}} = \frac{1}{n}\left(1 - \frac{1}{L}\right)\bar{\boldsymbol{F}}$ is used as the equivalent node load increment at each loading step. $\bar{\boldsymbol{F}}_i$ in eq. (76) can be obtained as follows:

$$\begin{aligned} \bar{\boldsymbol{F}}_i &= \frac{1}{L}\bar{\boldsymbol{F}} + i \cdot \Delta\bar{\boldsymbol{F}} = \frac{1}{L}\bar{\boldsymbol{F}} + i \cdot \frac{1}{n}\left(1 - \frac{1}{L}\right)\bar{\boldsymbol{F}} \\ &= \frac{n + i \cdot (L-1)}{nL}\bar{\boldsymbol{F}}, \quad (i = 1,\ 2,\ \cdots,\ n), \end{aligned} \tag{77}$$

where $n$ is total number of the loading steps.

## 5 Numerical examples

Two example problems are presented to demonstrate the applicability of the CVRKPM for two-dimensional elasto-plasticity problems. The results obtained for these examples using the CVRKPM are compared with the ones of the RKPM and ANSYS.

In the numerical examples presented in this section, the quadratic basis function is used in the construction of correction function, and the cubic spline weight function is used in the CVRKPM approximation. The rectangle zone is used as the support domain of nodes, and the scaling parameter $d_{\max}$ determining the size of the support domain is 3.5. The penalty factor is $\alpha = (1.0 \times 10^3) \times E$. In each integration cell, the 4×4 Gaussian quadrature is used for numerical integrations. And the total number of the loading steps for the examples in this section is $n$=100.

### 5.1 Cantilever beam subjected to a concentrated force

A cantilever beam subjected to a concentrated force at the free end is shown in Figure 1. In this example, the geometric parameters for this cantilever beam are as follows: the length of the beam is $L$=8 m, the height is $h$=1 m and

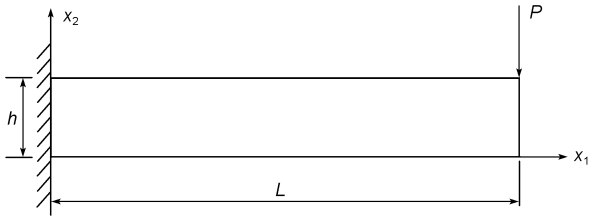


**Figure 1** Cantilever beam subjected to a concentrated force.

the depth is $t = 1$ m. The material properties are: the Young's modulus $E = 10^5$ Pa, the Poisson's ratio $v =$ 0.25, and the yield stress $\sigma_s = 25$ Pa. The linear hardening elasto-plastic model is adopted with $E' = 0.2E,$ and Mises yield criterion is used. The concentrated force is $P = 1$ N without gravity. And the plane stress problem is considered.

11×5 nodes are used, and the node distribution is shown in Figure 2. Using the CVRKPM presented in this paper we can obtain the displacement, stress and strain of the problem. The numerical solutions of vertical displacements at some nodes obtained using the CVRKPM are shown in Table 1. Compared with the numerical results obtained using the RKPM and ANSYS, we can see that the results using the CVRKPM are closer to those using ANSYS, and then the CVRKPM in this paper has a higher accuracy than the RKPM. And then under the same node distribution in the problem domain, the CVRKPM can improve the solution accuracy compared to the traditional RKPM.

The relationship between the displacements of midpoint at the end of the beam and the load is shown in Figure 3. It can be seen intuitively that when the load is larger than elastic limit, the material begins to yield and enters into the elasto-plastic state.

### 5.2 Perforated plate under an axial distributed load

The second example that is considered is a rectangular plate with a central hole under a distributed load, as shown in Figure 4. The length of the plate is $L = 10$ m, the width is $h = 4$ m, the radius of the central hole is $r = 1$ m, and the unit thickness of the plate is considered. The left end of the plate is fixed, and the distributed load $q = 1000$ N / m is applied at the right end of the plate. The other parameters used in our analysis are Young's modulus $E = 1.0 \times 10^5$ Pa, Poisson's ratio $v = 0.25,$ and the yield stress $\sigma_s = 250$ Pa.

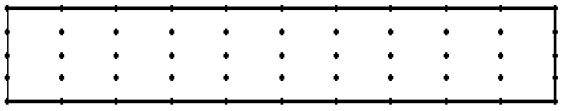

**Figure 2** Node distribution.

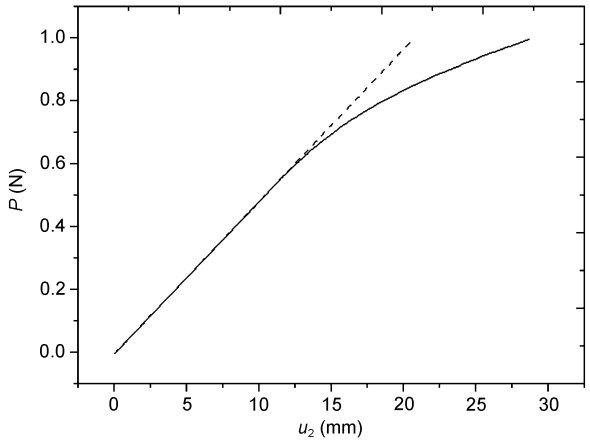


**Figure 3** Relationship between displacements of the midpoint at the end of the beam and the load.

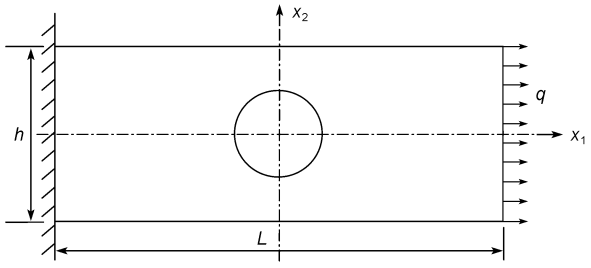


**Figure 4** A plate with a central hole under a distributed load.

The linear hardening elasto-plastic model is adopted with $E' = 0.2E,$ and Mises yield criterion is used.

As shown in Figure 5, 116 nodes in the domain are used for the solution. Other parameters are similar to those used in the first example in Section 5.1. The numerical results of displacements at some nodes using the CVRKPM and ANSYS are shown in Table 2. Similarly, it can be seen that the results obtained using CVRKPM show excellent agreement with those obtained using ANSYS. The relationship between the displacements of midpoint at the end of the beam and the load is shown in Figure 6. Similarly, when the

**Table 1** Vertical displacement of the beam subjected to a concentrated force (unit: mm)

| Node coordinate | | (1.6, 0.5) | (3.2, 0.5) | (4.8, 0.5) | (6.4, 0.5) | (8.0, 0.5) | The largest relative difference compared with ANSYS (%) |
|---|---|---|---|---|---|---|---|
| Elasticity solution | | 1.180 | 4.334 | 8.963 | 14.575 | 20.672 | |
| Elasto-plasticity solution | ANSYS | 2.020 | 6.837 | 13.227 | 20.600 | 28.460 | |
| | RKPM | 1.938 | 6.709 | 13.067 | 20.316 | 28.143 | 4.06 |
| | CVRKPM | 2.087 | 6.954 | 13.389 | 20.806 | 28.712 | 3.32 |

**Table 2** Elasto-plasticity solution of node displacement of the plate

| Node coordinate | $u_1$ (mm) | | $u_2$ (mm) | |
|---|---|---|---|---|
| | ANSYS | CVRKPM | ANSYS | CVRKPM |
| (–4.0,2.0) | 42.433 | 42.889 | 24.924 | 24.889 |
| (–3.0,2.0) | 84.524 | 83.872 | 27.557 | 28.471 |
| (–2.0,2.0) | 145.610 | 143.03 | 34.790 | 34.376 |
| (–1.0,2.0) | 225.550 | 220.14 | 77.695 | 75.728 |
| (0.0,2.0) | 274.670 | 267.25 | 126.600 | 117.962 |
| (1.0,2.0) | 323.040 | 313.20 | 76.718 | 74.658 |
| (2.0,2.0) | 403.350 | 391.37 | 34.099 | 33.361 |
| (3.0,2.0) | 466.270 | 451.45 | 27.784 | 28.275 |
| (4.0,2.0) | 512.480 | 497.51 | 30.547 | 30.235 |
| (5.0,2.0) | 552.920 | 537.79 | 32.323 | 32.225 |

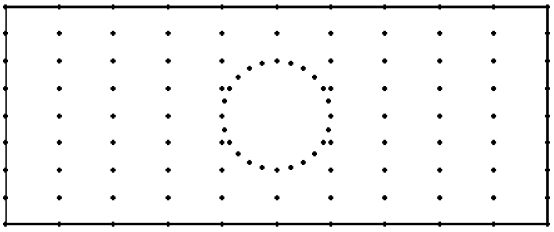

**Figure 5** Node distribution.

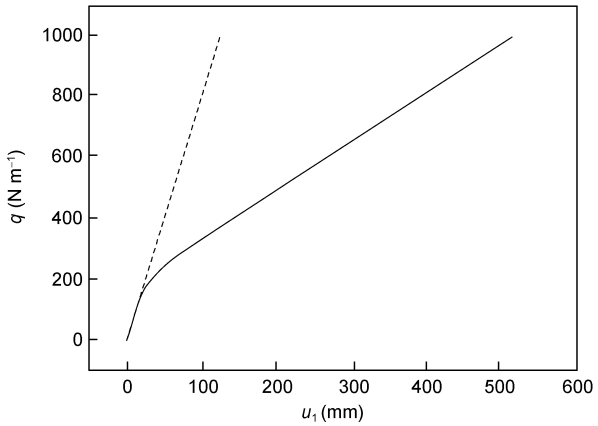


**Figure 6** Relationship between the displacements of the midpoint at the right end and the load.

load is larger than elastic limit, the material begins to yield and enters into the elasto-plastic state.

## 6 Discussion on the numerical accuracy of the CVRKPM

From many numerical examples, we analyze the effects of the size of the influence domain at a node, the number of nodes in the domain and the total number of the loading steps upon the numerical accuracy and computational efficiency, and obtain some similar conclusions. In this section, we give an example of the cantilever beam subjected to a distributed load to show some conclusions.

A cantilever beam subjected to a distributed load, as shown in Figure 7. The length of the beam is $L = 8$ m, the height is $h = 1$ m and the unit thickness of the plate is considered. This example is discussed as a plane stress problem. The distributed load is $q = 1\ \mathrm{N/m}$ without considering gravity. The other parameters used in our analysis are Young's modulus $E = 10^5$ Pa, Poisson's ratio $v = 0.25$, and the yield stress $\sigma_s = 25$ Pa. The linear hardening elasto-plastic model is adopted with $E' = 0.2E$, and Mises yield criterion is used.

### 6.1 Effect of the size of the influence domain upon the accuracy of the CVRKPM

Similar to the example in Section 5.1, a regular node arrangement of 11×5 is used, and the other parameters are also the same. The rectangle zone is still used as the support domain of node, and the scaling parameter $d_{\max}$ determining the size of the support domain can take the value of 2.0, 2.5, 3.0, 3.5, 4.0, 4.5, 5.0, 6.0 and 7.0, respectively. The corresponding numerical results using the CVRKPM are shown in Table 3. It can be seen that the size of the influence domain in the CVRKPM may have a certain effect upon the computational accuracy. For example, for the displacements of nodes at the axis of the beam, the computational accuracy is raised first and then drops slightly with the increasing value of $d_{\max}$, but the CPU time sustains to increase. Accordingly, as for the CVRKPM, taking two aspects of accuracy and CPU time into consideration, we think that the

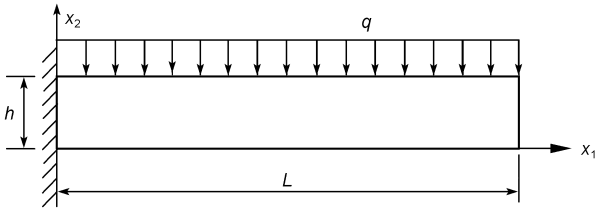


**Figure 7** Cantilever beam subjected to a distributed load.

**Table 3** Node displacement $u_2$ of cantilever beam under different influence domains

| Node coordinate | | (1.6,0.5) | (3.2,0.5) | (4.8,0.5) | (6.4,0.5) | (8.0,0.5) | Max relative difference compared with ANSYS (%) | CPU time (s) |
|---|---|---|---|---|---|---|---|---|
| ANSYS | | 18.279 | 60.587 | 113.12 | 167.96 | 223.19 | | |
| $d_{\max}$ | 2.0 | 16.957 | 57.495 | 108.12 | 160.99 | 214.24 | 7.23 | 161 |
| | 2.5 | 17.885 | 59.496 | 111.26 | 165.29 | 219.7 | 2.16 | 222 |
| | 3.0 | 18.15 | 59.989 | 111.97 | 166.23 | 220.88 | 1.03 | 293 |
| | 3.5 | 18.231 | 60.249 | 112.39 | 166.77 | 221.54 | 0.74 | 361 |
| | 4.0 | 18.295 | 60.398 | 112.6 | 167.05 | 221.89 | 0.58 | 432 |
| | 4.5 | 18.15 | 60.142 | 112.24 | 166.62 | 221.39 | 0.98 | 491 |
| | 5.0 | 18.058 | 60.017 | 112.01 | 166.37 | 221.11 | 1.21 | 535 |
| | 6.0 | 18.032 | 60.038 | 111.99 | 166.3 | 220.98 | 1.05 | 620 |
| | 7.0 | 17.905 | 59.841 | 111.64 | 165.88 | 220.5 | 2.05 | 692 |

value of parameter $d_{\max}$ is the most suitable when $3.5 \leqslant d_{\max} \leqslant 4.5$.

### 6.2 Effect of the node distribution on numerical accuracy of the CVRKPM

In this section, four kinds of regular node distribution are used for solution. The parameter $d_{\max}$=3.5, and the other parameters are the same as previously mentioned. The numerical results of displacements of nodes at the axis after the loading completion using the CVRKPM and ANSYS are shown in Figure 8. It can be seen that under different node distributions, the results of the CVRKPM all agree well with the results of ANSYS, but with the increase of the number of nodes, the numerical results of the CVRKPM can be better in agreement with those of ANSYS.

### 6.3 Influence of the number of the loading steps on numerical accuracy of the CVRKPM

Since the increment tangent stiffness matrix method is adopted in the CVRKPM for elasto-plasticity in this paper, the number of loading steps has an effect upon the numerical accuracy of the CVRKPM. Because load increment in each loading step is $\Delta\overline{\boldsymbol{F}} = \frac{1}{n}\left(1-\frac{1}{L}\right)\overline{\boldsymbol{F}}$, $n$ is the total number of the loading steps. Theoretically, the larger the total number of the loading steps is, the smaller the load increment will be. As a result, the numerical error, which is from the equations in the increment form when the equations in differential forms are replaced, will be smaller, and then the numerical accuracy of the CVRKPM will be higher. However, in the practical numerical process, the increasing of the total number of the loading steps will increase computational cost and reduce the computational efficiency. Therefore, it is a key problem to choose the total number of the loading steps to satisfy the requirements of numerical accuracy and efficiency.

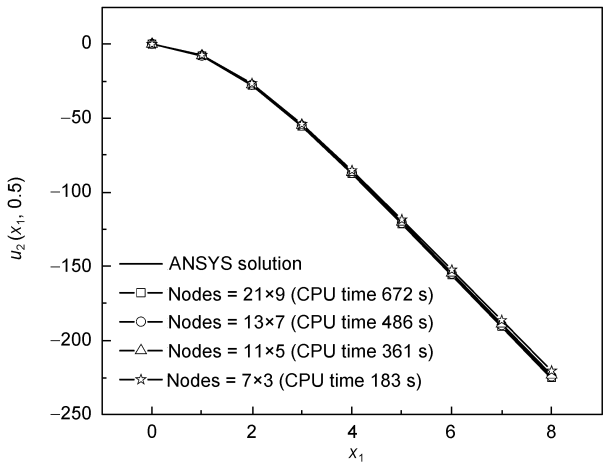


**Figure 8** Node displacements $u_2$ at the axis under different node distributions.

For the example in section 6.1, we choose the total number of the loading steps as 10, 30, 50, 70, 90, 100, 130, and 150, respectively. The node displacements $u_2$ of cantilever beam under different loading step numbers using the CVRKPM are shown in Table 4. It can be seen that the maximum relative difference is only 4.09% when the loading step number is 30, and this is because the Newton-Raphson method is used in this paper, and then the high numerical accuracy can be obtained when the total number of the loading steps is small.

The max relative difference of displacement of cantilever beam between the results using the CVRKPM and those using ANSYS depending on the loading step number is shown in Figure 9. It can be seen that the numerical accuracy will rise with the increase of the loading step number. But it can be seen again from Table 4 that the CPU time will increase, then the computing efficiency will be low. As a result, it is not necessary to choose a large number of the loading steps, otherwise the computational cost will increase greatly.

## 7 Conclusions

On the basis of the RKPM, the CVRKPM for elasto-plasticity problems is presented in this paper. The advantage of

**Table 4** Node displacement $u_2$ of cantilever beam under different loading step numbers

| Node coordinate | | (1.6,0.5) | (3.2,0.5) | (4.8,0.5) | (6.4,0.5) | (8.0,0.5) | Max relative difference compared with ANSYS solution (%) | CPU time (s) |
|---|---|---|---|---|---|---|---|---|
| ANSYS | | 18.279 | 60.587 | 113.12 | 167.96 | 223.19 | | |
| Loading step number | 10 | 16.363 | 54.69 | 102.08 | 151.55 | 201.41 | 10.48 | 41 |
| | 30 | 17.531 | 58.28 | 108.88 | 161.66 | 214.83 | 4.09 | 112 |
| | 50 | 17.894 | 59.428 | 110.96 | 164.71 | 218.85 | 2.11 | 185 |
| | 70 | 18.044 | 59.775 | 111.57 | 165.6 | 220.02 | 1.42 | 257 |
| | 90 | 18.139 | 60.051 | 112.06 | 166.31 | 220.95 | 1.0 | 328 |
| | 100 | 18.231 | 60.249 | 112.39 | 166.77 | 221.54 | 0.74 | 361 |
| | 130 | 18.402 | 60.643 | 113.03 | 167.66 | 222.68 | 0.67 | 473 |
| | 150 | 18.398 | 60.82 | 113.3 | 168.04 | 223.16 | 0.65 | 543 |

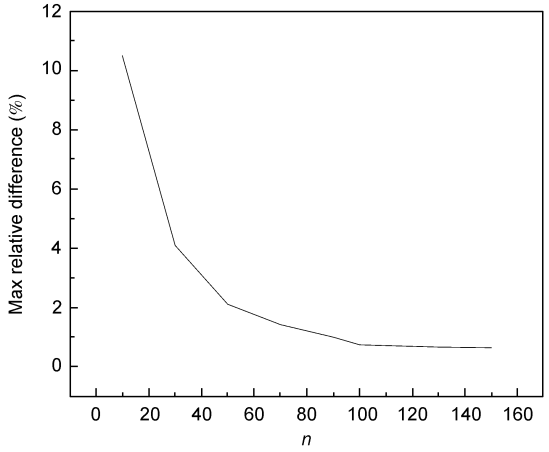


**Figure 9** Relationship between the max relative difference of numerical solution and the loading step number.

the CVRKPM is that the correction function of a 2D problem is formed with 1D basis function when the shape function is formed, and the approximation function of 2D problems is obtained further. And then the corresponding formulas of the CVRKPM for two-dimensional elasto-plasticity problems are derived. Some numerical examples are given. Compared to the solution using the RKPM and ANSYS, the present method is proved to be efficient.

In this paper, the effects of the size of the influence domain of the nodes, the total number of nodes arranged in the domain and the load step number upon the numerical precision and efficiency of the CVRKPM are discussed. And we obtained some conclusions: (1) The size of the influence domain of nodes can affect the results greatly, and the numerical precision of the CVRKPM will be great when the value of the scaling parameters $d_{\max}$ determining the size of influence domain of nodes is between 3.5 and 4.5; (2) the computational precision can be improved with the increase of the number of nodes distributed in the domain, but the CPU time will also increase correspondingly; (3) the computational precision can rise with the increase of the load step number, but the CPU time will increase greatly, and the computational efficiency will be decreased.

*This work was supported by the National Natural Science Foundation of China (Grant Nos. 10571118 and 10871124) and Innovation Program of Shanghai Municipal Education Commission (Grant No. 09ZZ99).*

1 Belytschko T, Krongauz Y, Organ D, et al. Meshless methods: An overview and recent developments. Comput Methods Appl Mech Eng, 1996, 139: 3–47
2 Li S F, Liu W K. Meshless and particles methods and their applications. Appl Mech Rev, 2002, 55: 1–34
3 Kargarnovin M H, Toussi H E, Fariborz S J. Elasto-plastic Element-free Galerkin Method. Comput Mech, 2003, 466–521
4 Chen Y, Eskandarian A, Oskard M, et al. Meshless analysis of plasticity with application to crack growth problems. Theor Appl Fract Mech, 2004, 41: 83–94
5 Kwon K C, Park S H, Youn S K. The least-squares meshfree method for elasto~plasticity and its application to metal forming analysis. Int J Numer Methods Eng, 2005, 64: 751–788
6 Long S, Chen S. Element-Free Galerkin method for elasto-plastic problems (in Chinese). Eng Mech, 2003, 20: 66–70
7 Xiong Y, Long S, Liu K. Analysis of the elasto-plastic problem by meshless method (in Chinese). J Mech Strength, 2004, 26: 647–651
8 Li W, Wang Y. Application of meshless method to elasto-plastic problems (in Chinese). Acta Mech Solida Sin, 2001, 22: 361–367
9 Zhao G, Song S, Yang X. Element-Free Galerkin method for elasto-plastic analysis based on incremental constitutive equations (in Chinese). J China Univ Min Technol, 2005, 34: 509–513
10 Belytschko T, Lu Y Y, Gu L. Element-free Galerkin methods. Int J Numer Methods Eng, 1994, 37: 229–256
11 Liu W K, Jun S, Zhang Y F. Reproducing kernel particle methods. Int J Numer Methods Eng, 1995, 20: 1081–1106
12 Duarte C A, Oden J T. An h-p adaptive method using clouds. Comput Methods Appl Mech Eng, 1996, 139: 237–262
13 Onate E, Idelsohn S, Zienkiewicz O C, et al. A finite point method in computational mechanics. Applications to convective transport and fluid flow. Int J Numer Methods Eng, 1996, 39: 3839–3866
14 Cheng R J, Cheng Y M. The meshless method for inverse heat conduction problem with a source parameter (in Chinese). Acta Phys Sin, 2007, 56: 5569–5574
15 Atluri S N, Zhu T. A new meshless local Petrov-Galerkin (MLPG) approach in computational mechanics. Comput Mech, 1998, 22: 117–127
16 Aluru N R. A point collocation method based on reproducing kernel approximations. Int J Numer Methods Eng, 2000, 47: 1083–1121
17 Liu W K, Chen Y J. Wavelet and multiple scale reproducing kernel methods. Int J Numer Methods Fluids, 1995, 21: 901–931
18 Idelsohn S R, Onate E, Calvo N, et al. The meshless finite element method. Int J Numer Methods Eng, 2003, 58: 893–912
19 Cheng Y M, Peng M J, Li J H. The moving least-square approximation with complex variables and its application in boundary element-free method for elasticity (in Chinese). Chin J Theor Appl

Mech, 2005, 37: 719–723
20 Cheng Y M, Li J H. A meshless method with complex variables for elasticity (in Chinese). Acta Phys Sin, 2005, 54: 4463–4471
21 Cheng Y M, Li J H. A complex variable meshless method for fracture problems. Sci China Ser G-Phys Mech Astron, 2006, 49: 46–59
22 Li S C, Cheng Y M. Meshless numerical manifold method based on unit partition (in Chinese). Acta Mech Sin, 2004, 36: 496–500
23 Li S C, Cheng Y M, Li S C. Meshless manifold method for dynamic fracture mechanics (in Chinese). Acta Phys Sin, 2006, 55: 4760–4766
24 Zhu T, Zhang J D, Atluri S N. A local boundary integral equation (LBIE) method in computational mechanics and a meshless discretization approach. Comput Mech, 1998, 21: 223–235
25 Kothnur V S, Mukherjee S, Mukherjee Y X. Tow dimensional linear elasticity by the boundary node method. Int J Solids Struct, 1999, 36: 1129–1147
26 Cheng Y M, Chen M J. A boundary element-free method for linear elasticity (in Chinese). Acta Mech Sin, 2003, 35: 181–186
27 Cheng Y M, Peng M J. Boundary element-free method for elastodynamics. Sci China Ser G-Phys Mech Astron, 2005, 48: 641–657
28 Qin Y X, Cheng Y M. Reproducing kernel particle boundary element-free method for elasticity (in Chinese). Acta Phys Sin, 2006, 55: 3215–3222
29 Dai B D, Cheng Y M. Local boundary integral equation method based on radial basis functions for potential problems (in Chinese). Acta Phys Sin, 2007, 56: 597–603
30 Chen L, Cheng Y M. Reproducing kernel particle method with complex variables for elasticity (in Chinese). Acta Phys Sin, 2008, 57: 1–10